ORIGINAL PAPER

A common source for the destructive earthquakes in the volcanic island of Ischia (Southern Italy): insights from historical and recent seismicity

Stefano Carlino[1] · Nicola Alessandro Pino[1] · Anna Tramelli[1] · Vincenzo De Novellis[2] · Vincenzo Convertito[1]

Abstract

The island of Ischia, located in the Gulf of Naples, represents an unusual case of resurgent caldera where small-to-moderate magnitude volcano-tectonic earthquakes generate large damage and catastrophic effects, as in the case of 4 March 1881 (I_{max}-VIII-IXMCS) and 28 July 1883 (I_{max} X-XI MCS) historical earthquakes, and of the recent 21 August 2017 MW = 3.9, event. All these earthquakes struck the northern area of the island. With about 65,000 inhabitants, Ischia is a popular touristic destination for thermals baths, hosting more than 3,000,000 visitors per year, thus representing a high seismic risk area. Assessing its seismic potential appears a fundamental goal and, to this end, the estimate of the magnitude of significant historical events and the characterization of their source are crucial. We report here a reassessment of historical data of damage of 1881 and 1883 earthquakes to evaluate the main source parameters of these events (obtained with the BOXER and EXISM software) and quantitatively compare, for the first time, the results with the source characteristics, obtained from instrumental data, of the recent 2017 earthquake. The results allowed us to assess the location, as well as the possible dimension and the related maximum magnitude, of the seismogenic structure responsible for such damaging earthquakes. Our results also provide an additional framework to define the mechanisms leading to earthquakes associated with the dynamics of calderas.

Keywords Macroseismic · Intensity · Casamicciola · Ischia Island · Historical and instrumental earthquakes · Subsidence · Caldera

✉ Stefano Carlino
  stefano.carlino@ingv.it

1   INGV-Istituto Nazionale di Geofisica e Vulcanologia, Sezione di Napoli-Osservatorio Vesuviano, Via Diocleziano, 328, 80124 Napoli, Italy

2   IREA-CNR Istituto per iI Rilevamento Elettromagnetico dell'Ambiente, Naples, Italy

1 Introduction

The seismicity of active volcanic areas is generally characterized by low magnitude earthquakes (McNutt and Roman 2015). Nevertheless, the occurrence of moderate ($4 < M < 5$) volcano-tectonic events is not rare and can generate damage and fatalities (Zobin 2012), mainly due to their shallow hypocentral depth (e.g. Convertito and Zollo 2011). Volcano-tectonic earthquakes are mostly associated with the magma dynamic but, in some cases, could be not straightforwardly correlated to primarily magmatic processes. A well-known case is the active volcanic island of Ischia (located in the Gulf of Naples), where recent and historical earthquakes have caused heavy damage and thousands of fatalities (Cubellis and Luongo 1998; Carlino et al. 2010) (Table 4, Appendix) (Fig. 1). These events appear to be associated with a phase of subsidence of the central part of the island (Trasatti et al. 2020).

Ischia is a 46 km^2 island located a few km west of Naples. It is an active resurgent caldera, whose central part underwent large uplift, about 900 m since ~ 55 ka (Sbrana et al. 2009), and subsidence in historical time (Buchner et al. 1996; Manzo et al. 2006). The resurgence generated the Mt. Epomeo block, an approximately ~ 2×2 km^2 squared structure, bordered by a system of faults mainly oriented NW–SE, E-W, and N-S (Fig. 1). The resurgence was accompanied by volcanic activity outside the block (last eruption in 1302) and produced the exhumation of a high-temperature hydrothermal system, with geothermal gradients > 150 °C km^{-1} (Vezzoli 1988; Sbrana et al. 2009; Sbrana and Toccaceli 2011; Carlino 2018).

During the nineteenth century, the island of Ischia was a very important site for the Earth Science scholars and one of the most famous places for spas in Europe (Carlino, 2019). For these reasons, many accounts and reports were produced after the earthquakes of 4 March 1881 and 28 July 1883. In particular, many coeval papers, technical reports, and various accounts described the damage distribution of these two events (see Cubellis and Luongo 1998, and references therein), leading to the assessment of macroseismic intensity of I_0 VIII-IX MCS and I_0 X-XI MCS, respectively, for the 1881 and the 1883 earthquakes (Cubellis and Luongo 1998; Cubellis et al. 2004; Carlino et al. 2010). Intensity data (EMS98) for both earthquakes are included in the Parametric Catalogue of Italian Earthquakes (CPTI15, Rovida et al. 2019). In particular, the CPTI15 lists 17 (11 on the island) and 27 (18 on the island) intensity–points (localities) for the 1881 and the 1883 earthquakes, respectively, for which the epicentral intensity (I_0) IX EMS98 (1881) and X EMS98 (1883) are reported.

With more than 2300 victims and the whole destruction of the town of Casamicciola Terme, the 1883 event was the most devastating (Carlino et al. 2010). Considering the small-to-moderate magnitude inferred from previous studies (e.g. $4.6 \leq M \leq 5.2$; Cubellis and Luongo 1998), the high damaging level of this earthquake can be primarily related to the shallowness of the seismogenic source, which is located between 1 and 2 km of depth (Cubellis and Luongo 1998; Carlino et al. 2010).

As for the whole of Italy (Crescimbene et al. 2015), seismic risk has not been adequately perceived by the inhabitants of the island, until 21 August 2017 when a $M_d = 4.0$ ($M_W = 3.9$) earthquake stroke the island. The occurrence of this recent earthquake, after 134 years of almost complete seismic silence, has brought out again the problem of the relatively high seismic risk for the island (Briseghella et al. 2019; De Natale et al. 2019; Marotta et al. 2019). Based on the current national seismic hazard map provided by the Istituto Nazionale di Geofisica e Vulcanologia (http://esse1.mi.ingv.it/), for the whole island the acceleration with probability of exceeding equal to 10% in 50 years ranges between 0.125 and 0.175 g

(being *g* the gravity acceleration and the values corresponding to the 50th percentile) with a range of variability (0.1, 0.2) *g* (corresponding to the 16th and 84th percentile, respectively). In fact, given the grid at which the national hazard map is computed there are only two points for the entire island. In this regard, the 2017 earthquake was the first significant event at Ischia recorded instrumentally, for which a PGA of 0.25 g was recorded at about 800 m from the epicentre (De Novellis et al. 2018). Although the comparison between the recorded value and the expected values indicated in the national seismic hazard should take into account the probabilistic nature of the latter and its reference to bedrock soil condition, we note that the recorded value is larger than the expected value at the 84th percentile.

The source mechanism of the 2017 earthquake has been differently interpreted by various authors (De Novellis et al. 2018; Braun et al. 2018; Calderoni et al. 2019; Nazeri et al. 2020). As for the 1881 and 1883 events, albeit to a limited extent, this last earthquake produced serious destruction in spite of its modest magnitude, causing two fatalities, more than 40 injuries and serious damage in the upper part of the town (Nappi et al. 2018). Before its occurrence, only about 50 very-low magnitude earthquakes ($M < 2.3$) had been recorded since 1999 by the seismic network installed on the island. Despite the seriousness of the situation, the 2017 event gave us the opportunity to deepen our understanding of seismic processes occurring in the island, comparing the latter event to the historical ones, which seem to have similar characteristics.

In this study, we compare for the first time the macroseismic data of two main historical earthquakes of Ischia (1881, 1883) to those of the first instrumental earthquake occurred in the island in 2017. This represents a first important step to quantitatively compare macroseismic and instrumental events for the study of the seismic source of this volcanic area. We use uniform and standard criteria to represent the macroseismic field and to retrieve the fault parameters of the three events, in order to analyse the location and the kinematic of the seismogenic structures generating highly damaging earthquakes in the island, verifying their relation and/or their possible coincidence. In particular, we elaborated the intensity data of both the 4 March 1881 and the 28 July 1883 earthquakes, which are mainly inferred from the analysis of historical archive reports. We reassessed the data for the 1881 and 1883 earthquakes following macroseismic criteria and using the EMS98 scale, to obtain macroseismic fields. We inferred new magnitude estimations and retrieved the geometry of the faults using different computational methods: BOXER (Gasperini and Ferrari 2000; Gasperini et al. 1999) and EXSIM (Motazedian and Atkinson 2005; Boore 2009; Assatourians and Atkinson 2012). Then, we compared the results to the fault plane solution and the damage of the 21 August 2017 earthquake. The results suggest the presence of a unique seismogenic structure, which can be periodically reactivated during the present quiescent phase of the volcano, providing new elements to assess the processes that could generate earthquakes in subsiding calderas. Noteworthy, the fault geometries obtained in the present study can also help to refine the seismic hazard estimates for the island, in particular for those approaches based on single faults rather than areal seismic source zones (e.g. Akinci et al. 2009; Convertito et al. 2006; Pace et al. 2006).

2 Historical Data

The description of the damage of the 1881 and 1883 earthquakes and the felt report data had been previously reported in various papers and databases (Cubellis and Luongo 1998; Cubellis et al. 2004; Carlino et al. 2010; Rovida et al. 2019). Those data had been

elaborated by various authors to provide an estimation of epicentral intensity, epicentral location, and intensity-related magnitude (see for instance Cubellis and Luongo 1998; Carlino et al. 2010, and Rovida et al. 2019).

The macroseismic intensities of the 1883 event published by Cubellis and Luongo (1998), Cubellis et al. (2004) and Carlino et al. (2010) have been obtained by assigning the intensity value to very small localities, represented by a group of edifices located in a single street or district. This procedure does not match with the standard macroseismic method (see, for instance, Grünthal 1998, Musson et al. 2008, and Locati et al. 2019), because in many cases the intensity was assigned according to damage suffered by a too low number of edifices that is not representative for an intensity estimate. On the other hand, in the CPTI15 (Rovida et al. 2019), the number of intensity points represented on the Ischia Island for each one of the three considered earthquakes differs significantly (11 points for the 1881, 17 for the 1883, 24 for the 2017). In particular, the CPTI15 reports a lower number of points in the highest damage (and densely inhabited) areas for the 1881 and 1883 earthquakes with respect to 2017. Given the very shallow hypocentre depth of these events (generally associated with very fast spatial variation of the intensity) and pointing at retrieving more information on their source characteristics, our first intent was to homogenize the areal coverage of the intensity points of 1881 and 1883 events, to get a distribution comparable with that of 2017. In particular, the macroseismic intensities for the 1881 and 1883 earthquakes can be reviewed on the basis of the large amount of available data.

In general, the analyses of seismic intensity data represent the only way to retrieve information about the location and the dimension of the seismogenic source of seismic events occurred in the pre-instrumental era (e.g. Panza and Cuscito 1982; Gasperini and Ferrari 2000; Gasperini et al. 1999; Tertulliani et al. 2012). However, these methods are affected by a number of uncertainties, also due to the local geological conditions, affecting the seismic wave propagation and amplification, and to the different seismic response of the buildings. However, the above uncertainties can be reduced in the case of the 1881 and 1883, in consideration of the quality and quantity of available historical data.

Considering the moderate magnitude of the events, the observed very fast decay of the damage level (that is, the fast spatial variation of intensities) would require a higher level of detail of the intensity pattern with respect to larger earthquakes, to retrieve information on the source characteristics. Thus, we collected the original descriptions of the damage, for both the earthquakes, and increased the number of data points in the northern zone of the island, which was affected by larger damage.

For the 1883 event, we used the original description of the damage, derived from the consultation of the report of the *Comitato Centrale di soccorso pei dannegiati dell'isola d'Ischia* (1885) (Rescue Committee for the damage of the island of Ischia), which represents the most detailed data source for the damage caused by this event. Immediately after the events, the Committee provided technical forms with the description of damage suffered by each building (with indication of the street and, when available, of the building number) (see also Cubellis et al. 2004 and Carlino et al. 2010).

We grouped the original damage data by location, prior to assessing intensity, as recommended by Musson et al. (2008). We used the criteria for which a location is represented by multiple settlements (MS) (Locati et al. 2019), which is a significant number of buildings grouped in a well-known site. The locations are distributed within the six different municipalities of the island (Casamicciola, Lacco Ameno, Forio, Serrara Fontana, Barano, Ischia). Apart from a few exceptions regarding non-damaged zones, we considered only the MS having a number of buildings > 50 units. The report of the *Comitato Centrale pei*

Dannegiati dell'isola d'Ischia (1885) also includes damage data of the island for the 1881 earthquake. However, due to the limited information, we also consulted further literature data (see Cubellis and Luongo 1998, and references therein). We adopted the same criteria used for the 1883 event in the identification of the localities, finally obtaining intensity data for the 1881 earthquake.

In the end, damage data for about 3000 edifices (total) located in the island were analysed. Furthermore, surface effects, such as major fractures, open-cracks and landslides have been also considered in the evaluation of the intensity, taking into account the contemporary chronicles and technical reports (see Cubellis and Luongo 1998, and references therein). On the base of the damage descriptions, we evaluated the EMS98 intensity for the 1881 and 1883 earthquakes, obtaining intensity data for 20 (Table 5, Appendix) and 26 (Table 6, Appendix) locations on the island, respectively, assigning a name to each MS on the basis of the present toponymy (Grünthal 1998). In Fig. 8 of Appendix, we also report the different intensity maps (1881 and 1883) in which the distribution of our intensity points is compared with those reported in the CPTI15 (Rovida et al. 2019).

As for the vulnerability classification (Grünthal 1998) for Ischia Island, apart for a few noble buildings, at the end of nineteenth century, the building heritage of the island was mainly made by the same local tuff masonry, with local rough stone and/or squared stony blocks (Polverino 1996, 1998; Cubellis and Luongo 1998), all belonging typologies to vulnerability class B. Also, recent studies report that (at least in the most damaged area) the building heritage erected before the 1919 mainly falls in the vulnerability class B and C and only in minor part to class A (~ 12% and ~ 25%, respectively, for the Lacco Ameno and the Casamicciola Terme municipalities; Verderame et al. 2017; Del Gaudio et al. 2018). The poor building typology might have increased the overall damage. In fact, many locations of the northern sector of the island (between Casamicciola Terme and Lacco Ameno municipalities) fall in the damage classification 3 to 5 (damage from "significant" to "very heavy"), while the damage were heavy at the epicentre (Casamicciola Terme) for both the earthquakes (1881, 1883). In the municipality of Casamicciola Terme, 250 edifices out of about 800 suffered heavy damage during the 1881 event, and about 670 were collapsed during the 1883 earthquake (*Comitato Centrale pei dannegiati dell'isola d'Ischia, 1885)* Furthermore, the similarity of the poor architectural technique in the whole island, possibly contributed to a general increase of damage, and not in its difference in the spatial distribution (Polverino 1998). Finally, it should be stressed that the damage produced by the 1881 earthquake had probably weakened the buildings stock, contributing to an increase of the effects during the following 1883 event. Anyway, due to the lack of punctual information of the 1881, this cannot be quantified in terms of increase of vulnerability.

Fig. 2 depicts the macroseismic field of 1881 and 1883 earthquakes, obtained from the interpolation of the intensities data listed in Appendix Tables 5 and 6, and the 2017 macroseismic field from CPTI15 (Rovida et al. 2019) data (we used the kriging method for the interpolation of data; Kerry and Hawick, 1998).

3 Assessment of the modelling approach

3.1 Direct modelling of the 2017 earthquake

To infer the geometry and the orientation of the faults responsible for the two historical 1881 and 1883 earthquakes, we implemented a procedure similar to that proposed by

Convertito and Pino (2014) to study the 1908 Messina Straits earthquake. We first selected a set of parameters for model faults in terms of orientation (strike and dip), Mach number values (i.e. the ratio between rupture velocity and shear-wave velocity), and static stress drop. Then, for each model, we computed peak-ground acceleration (PGA) and peak-ground velocity (PGV) by using the EXSIM code (Assatourians and Atkinson 2012; Atkinson and Assatourians 2014) at the geographic locations where the observed macroseismic intensities are available. The computed PGAs and PGVs are finally converted to macroseismic intensities by using the relationship proposed by Faenza and Michelini (2010) and compared with the observed ones. The best model corresponds to the one that minimizes the misfit function:

$$f(\boldsymbol{m}) = \sum_{i=1}^{N} \frac{\left(I_i^{\text{obs}} - I_i^{\text{cal}}\right)^2}{I_i^{\text{cal}}} \tag{1}$$

In Eq. (1), $\boldsymbol{m}$ is the model parameters' vector, whose components are the length L and the width W of the fault, its strike and dip, the stress drop ($\Delta\sigma$), and the Mach number (α). N is the number of intensity data points, I_i^{obs} are the observed intensities and I_i^{cal} are the intensities obtained from PGAs or PGVs.

Before analysing the two historical earthquakes, in order the check the performance of the whole procedure, we tested the method on the recent 21 August 2017 ($M_w = 3.9$) earthquake that stroke the same area and for which a reliable model exists for its source geometry and slip distribution (De Novellis et al. 2018). We examined both the direct and the inverse modelling. As for the direct problem, we first computed the predicted intensities from PGAs and PGVs obtained for a realistic source model and checked the results against the observations. Then, as for the inverse problem, we computed intensities for distinct simplified source models and used the observed intensities to determine the source characteristics better simulating the data and compared the best solution with the actual source.

In all the EXSIM computations, we assumed a crustal model characterized by average S-wave velocity value of 1700 m/s, density of 2700 kg/m^3, and a frequency-dependent anelastic attenuation model $Q(f) = 21f^{0.6}$ (being Q the quality factor and f the frequency) (Nunziata and Rapolla 1987; Petrosino et al. 2008; Del Pezzo and Bianco 2013; Capuano et al. 2015). Given the relatively short source-to-site distances considered in this study, a 1/R geometrical spreading is considered (where R is the minimum site distance from the fault). The fault plane was assumed to be rectangular and was subdivided into an appropriate number of 0.1×0.1 km^2 sub-faults, which are modelled as point sources characterized by a ω^{-2} spectrum. The upper left corner of the fault is used as reference fault point (Assatourians and Atkinson 2012; Atkinson and Assatourians 2014). Moreover, in the simulations, we always investigated three stress-drop values (0.1, 1, and 3 MPa), as typical ranges for volcanic areas (e.g. De Natale et al. 1987, 1988) and three Mach number values (0.6, 0.7, and 0.8), as reasonable range for light-to-moderate earthquakes (e.g. Seekins and Boatwright 2010; Convertito et al. 2012).

As for local effects, previous studies suggest that in the northern sector of the island the effect of seismic waves propagation, as well as site amplification, can be considered less important with respect to source effects, because of both the very shallowness of the hypocentre and the relatively short hypocentral distances (Cubellis and Luongo 1998; Gasperini and Ferrari 2000). Also, recent seismic measurements performed in the most damaged area of the 2017 earthquake conclude that H/V spectral analyses performed on seismic noise do not show important peaks related to site amplification (Vassallo et al. 2018). On the other

hand, microzonation investigations in three municipalities, in the northern and western areas of the island, determined amplification factors in the range 1 to 3 for the frequency band of interest (1.25–10 Hz) (http://www.commissarioricostruzioneischia.it/Esiti-Micro zonazione.html). Unfortunately, the three districts only cover a limited extent of the island and less than 50% of the data points. On these grounds, we cannot account quantitatively for the site effect, unless assigning arbitrary values to all the sites with unknown site amplification factor. Thus, we simulated PGAs and PGVs at the bedrock.

Firstly, for the direct modelling of the 2017 earthquake, we adopted the fault geometry (L × W = 3.0 × 1.8 km^2; fault strike 86° ± 5°; dip angle 70° ± 7°) inferred from the analysis of DinSAR data by De Novellis et al. (2018) and their slip distribution, characterized by a single patch with most slip confined approximately in a 0.5 km-radius circle. We used the observed macroseismic field available in the CPTI15 parametric catalogue (Rovida et al. 2019), consisting of 24 intensity data points ranging between III and VIII. For both PGA and PGV, we obtained the best solutions for Δσ = 1.0 MPa and α = 0.7 (Fig. 3 and Model M1-A-B in Table 1), and maximum PGA and PGV value of about 0.5 m/s^2 and 0.16 m/s, respectively. Notably, PGA-derived intensities definitely provide a better fit with the hypocentral distance with respect to PGV. This result can be ascribed to the very short source-to-site distances and to the fact that the considered event is a low magnitude one, with a major relative contribution of high frequencies to the peak-ground motion. Based on this test, we considered the PGAs better able to reproduce the data and, thus, to provide a more robust link between the source fault and the observed intensities.

To test the effects of our assumptions on the local amplification, we modified the PGAs and PGVs obtained for the best model and the "true" slip distribution and fault geometry, considering the relevant amplification factors. In particular, we applied amplification factors in the frequency bands 2–10 Hz and 1.25–2.5 Hz, respectively, to PGA and PGV. As obvious, this could be done only for the sites for which the factor is available (squares in Fig. 3). Remarkably, only for three of the tested sites the resulting intensity is 0.66 larger than the value obtained from PGA and PGV at the bedrock and, most important, the modified values provide comparable (0.120 vs. 0.117, for PGA) or worse (1.2259 vs. 0.268, for PGV) fit to the observed intensities.

3.2 Inverse modelling of the 2017 earthquake

In order to investigate how much of a realistic source can be retrieved from the modelling of macroseismic data points, we applied an inverse approach by assuming for the 2017 earthquake the observed intensities. We initially used the CPTI15 epicentre (Rovida et al. 2019) and the fault azimuth and extent resulting by using BOXER code (Gasperini and Ferrar 2000; Gasperini et al. 1999, 2010), obtaining 80.50° (± 31°) and 0.8 × 1.9 km^2, respectively. Then, we assumed uniform slip distribution and, by slightly varying the parameters, searched for the best fault by converting the EXSIM predictions to intensity and comparing these latter with the observed ones. In particular, we used the EXSIM results to test the sensitivity of the intensity data points to fault length and also checked the possibility of the whole procedure to retrieve the fault dip. We investigated three fault surfaces extents (1 × 1, 2 × 2, 3 × 3 km^2), with the top in correspondence of the Earth surface, and two opposite fault strike directions (80.50° and 260.50°). In the lack of any constraints about the hypocentre, we fixed it at half-length along the strike and 0.2 km above the fault bottom (e.g. Mai et al. 2005). As for the dip angle, the major faults on the island are all vertical or subvertical (Acocella and Funiciello 1999; Vezzoli 1998; Sbrana and Toccaceli 2011) thus, for

Table 1 Best solutions for the investigated models for the August 27, 2017, $M_d = 4.0$, earthquake

Model	Strike (°)	Dip (°)	Δσ (MPa)	L (km)	W (km)	α	X (km)	Y (km)	Misfit
M1A	86	70	0.1	3.0	1.8	0.7	1.5	1.6	0.117
M1V	86	70	0.1	3.0	1.8	0.7	1.5	1.6	0.268
MB17A	80	70	0.1	1.0	1.0	0.6	0.5	0.8	0.106
MB17V	80	70	0.1	2.0	2.0	0.6	1.0	1.8	0.208

X and Y indicate the position of the nucleation point on the fault plane along the strike and along the dip, respectively, and α if the Mach number. M1 is the source model of De Novellis et al. (2018), while MB17 represents the best solutions obtained starting from the BOXER result for the 2017 earthquake and assuming uniform slip. For each model, A and B refer to the results obtained computing PGA and PGV, respectively
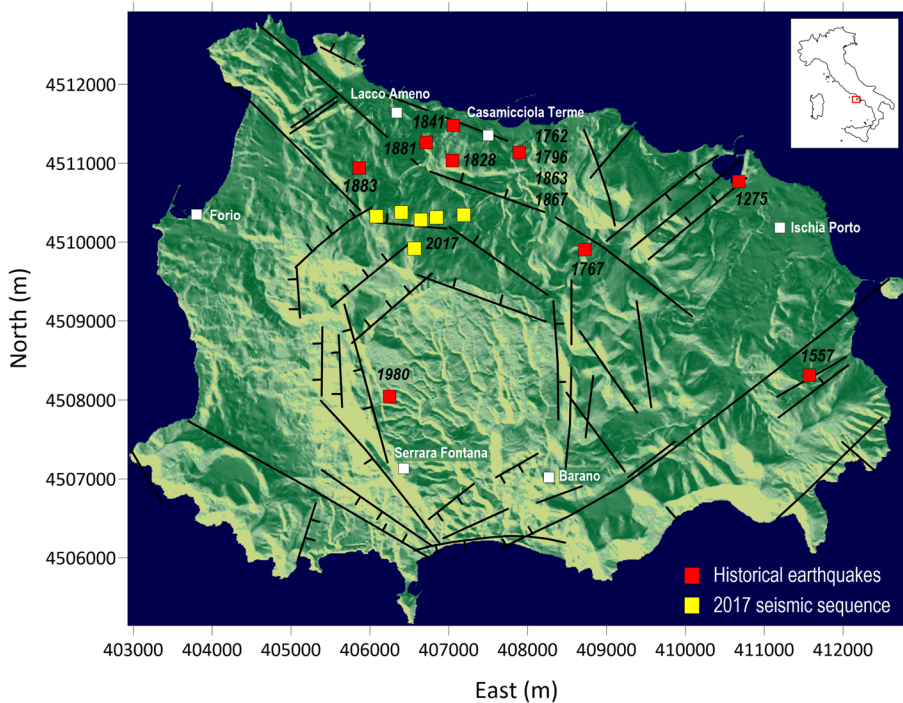

Fig. 1 The Island of Ischia and the most significant seismicity. Black lines are the main fault systems of the island (after Sbrana and Toccaceli 2011). The historical earthquakes epicentres are taken from the CPTI15 (Rovida et al. 2019) while the location of most recent 2017 seismic swarm is from INGV seismic database (Modified after De Novellis et al. 2018)

each combination of fault strike and fault extent we computed synthetic intensities for two fault dips, 70° and 90°, with the two strikes giving coincident faults for the vertical planes.

The best model is illustrated in Fig. 4 and listed in Table 1 (MB17). As expected from the previous test, the PGA-derived intensities simulate the data significantly better then PGVs. Both PGAs and PGVs indicate 80.50° as preferred strike and stress drop Δσ = 0.1 MPa. However, while PGAs prefer a small, vertical fault (1×1 km²) with Mach number α = 0.7, PGVs are better simulated by using a larger fault (2×2 km²) dipping 70°

and with slightly lower rupture velocity ($\alpha = 0.6$). Considering the assumption of uniform dislocation and the slip distribution derived from the DInSAR analysis (De Novellis et al. 2018), the smaller fault extent appears to be in better agreement with the geodetic solution. Finally, the difference in the fault dip angle between the two preferred solutions can be considered as an estimate of the uncertainty for this parameter. The maximum PGA and PGV values are 0.5 and 0.32 m/s, respectively.

Based on the above observations, we deemed the modelling of the PGA-derived intensities more reliable in determining the source geometry and used the PGVs anyway to evaluate the robustness of the preferred solution.

4 Results

4.1 Magnitude estimation of 1881 and 1883 events

In order to proceed with the simulations for the 1881 and 1883 earthquakes, we first assessed the magnitude of these events, which have been used together with the other parameters, as input data of BOXER. Different intensity-magnitude relations have been already used for the 1883 earthquake and provide a magnitude range between 4.6 and 5.2 (Cubellis and Luongo 1998 and references therein). After the 2017 earthquake, we could have a first instrumental assessment of the magnitude for a significant earthquake at Ischia ($M_d = 4.0$, $M_W = 3.9$; http://cnt.rm.ingv.it), which can be compared with its maximum intensity (I_0 EMS98 VII-VIII) (Rovida et al. 2019). Thus, among the most used intensity-magnitude relationships for volcanic areas (Patanè et al. 1986; Marturano et al. 1988; Azzaro et al. 2011) (Table 2), we used the ones that provide the most consistent result for the 2017 event. Considering I_0 EMS98 VII-VIII, the intensity-magnitude relationships that provides the closer values to $M_W = 3.9$ (or $M_d = 4.0$) are that derived by Patanè et al. (1986), giving M = 3.8, and the one proposed by Azzaro et al. (2011), giving $M_{d(average)} = 3.8$. On the other

Table 2 Magnitude estimation for the 1881, 1883 and 2017 Casamicciola earthquakes, using different I_0-M (maximum intensity-magnitude) relationships (Patanè et al. 1986; Marturano et al. 1988; Azzaro et al. 2011)

Relation	Reference	I_0*	Value (M)			Earthquake
$M = 0.4 I_0 + 0.8$	Patanè et al. (1986)	(VIII-IX)	4.2			1881
		(X-XI)	5.0			1883
		(VII-VIII)	3.8			2017
$M = (\log I_0\_0.155)/(0.165)$	Marturano et al. (1988)	VIII-IX	4.6			1881
		X-XI	5.1			1883
		VII-VIII	4.3			2017
			$M_{d(min)}$	$M_{d(average)}$	$M_{d(max)}$	
$M_d = 0.31(\pm 0.03)$ $I_0 + 1.51(\pm 0.14)$	Azzaro et al. (2011)	VIII-IX	3.8	4.1(± 0.12)	4.5	1881
		X-XI	4.3	4.8(± 0.12)	5.2	1883
		VII-VIII	3.5	3.8(± 0.12)	4.2	2017

See text for details

*According to Gasperini and Ferrari (1990), Gasperini et al. (1999) and Gasperini et al. (2010) the value I_0 for the magnitude assessment is the average of the two maximum values of the epicentral area

side, the result of the magnitude-intensity relation of Marturano et al. (1988) (Table 2) provides a difference with respect to the 2017 M_d and M_W of 0.4 and 0.3, respectively. This difference is larger or at the limit of the uncertainty in the evaluation of the magnitude of 2017 earthquake (± 0.3; http://cnt.rm.ingv.it), thus we excluded this relation from the following computations. By applying the relations proposed by Patanè et al. (1986) and Azzaro et al. (2011), we obtained $M = 4.2$ and $M_{d(average)} = 4.1$, for the 1881 event, and $M = 5.0$ and $M_{d(average)} = 4.8$, for the 1883 event, respectively (Table 2). However, we notice that, compared to that inferred by Patanè et al. (1986), the relation proposed by Azzaro et al. (2011) is better constrained, being inferred from an about fivefold number of earthquakes. Thus, in the next steps, we utilized the relation derived by Azzaro et al. (2011).

4.2 Retrieved faults parameters for the 1881 and 1881 events

Concerning the 4 March 1881 earthquake, we used the macroseismic intensities obtained in the present study consisting of 20 intensity points ranging between IV and IX. We first used BOXER to infer the best macroseismic epicentre and surface fault projection extent. We obtained 40.744°N (± 0.2 km) 13.903°E (± 0.4 km) for the epicentral location, very close to that obtained for the 2017 event, a best azimuth of 88° ($\pm 30°$), and fault extent 1×2 km^2. Next, following the same approach used above for the 2017 event, we computed PGAs and PGVs and converted them to macroseismic intensities. We tested two opposite strikes (88° and 268°), two dips (70° and 90°), three fault geometries (1×1, 2×2, 3×3 km^2), three stress-drop values (0.1, 1, 3 MPa), and three Mach number values (0.6, 0.7, 0.8). For the historical events, considering the uncertainty in the BOXER epicentral location, we also tested different reference points, by moving it ± 500 m along the N-S direction and, for each one of these two locations, also shifting it ± 500 m along the direction identified by the azimuth obtained from BOXER. We used uniform slip distribution for all the investigated models.

The best models for PGA and PGV are represented in Fig. 5 and listed in Table 3 (MB81A and MB81V). Like for the 2017 event, a lower misfit results for PGA. Both PGA- and PGV-derived intensities indicate a 2×2 km^2 fault plane, with Mach number $\alpha = 0.6$ and stress drop $\Delta\sigma = 1$ MPa. The stress drop is larger than what obtained for the 2017 event, possibly reflecting the higher maximum intensity of the 1881 earthquake with respect to what estimated for 2017. In contrast, different fault dips result for PGA and PGV, respectively, with the former dipping 70° and the latter being a purely vertical plane. The two planes have the same fault centre, which is slightly shifted (500 m) to the south and to the west relative to the BOXER solution. This disparity may result from the different assumption of the two inversion schemes: BOXER uses only the

Table 3 Best solutions for the investigated models for the 4 March 1881, $M_W = 4.1$, earthquake (MB81A and MB81V) and for the 28 July 1883, $M_W = 4.8$, earthquake (MB83A and MB83V)

Model	Strike (°)	Dip (°)	$\Delta\sigma$ (MPa)	L (km)	W (km)	α	X (km)	Y (km)	Misfit
MB81A	88	70	1.0	2	2	0.6	1.0	1.8	7.37E−2
MB81V	88	90	1.0	2	2	0.6	1.0	1.8	9.52E−2
MB83A	86	90	1.0	1	1	0.6	0.5	0.8	5.98E−2
MB83V	266	70	1.0	2	2	0.8	1.0	1.8	7.61E−2

X and Y indicate the position of the nucleation point on the fault plane along the strike and along the dip, respectively, and α if the Mach number. For each model, A refers to the results obtained when computing PGA and V when computing PGV
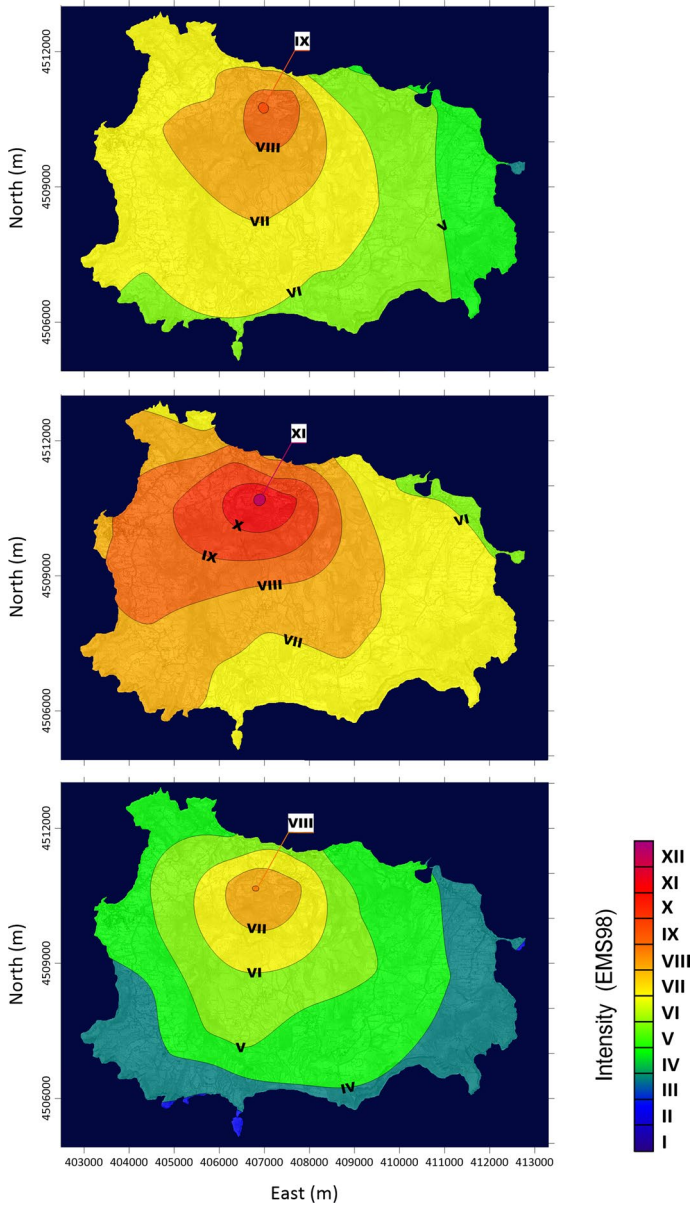
Fig. 2 Macroseismic field of 1881 (**top**), 1883 (**center**) and 2017 (**bottom**) earthquakes obtained from the interpolation of the intensities data listed in Tables 5 and 6 (1881 and 1883) and the intensity data from CPTI15 (2017) (Rovida et al. 2019) (see text for details)

points corresponding with the major intensities, while the synthetic intensities obtained through EXSIM are compared to all the data points on the island. In fact, the observed macroseismic field of the 1881 earthquake is characterized by a clear asymmetry, with rapidly decreasing intensity moving eastward from I_0, while higher values are located in
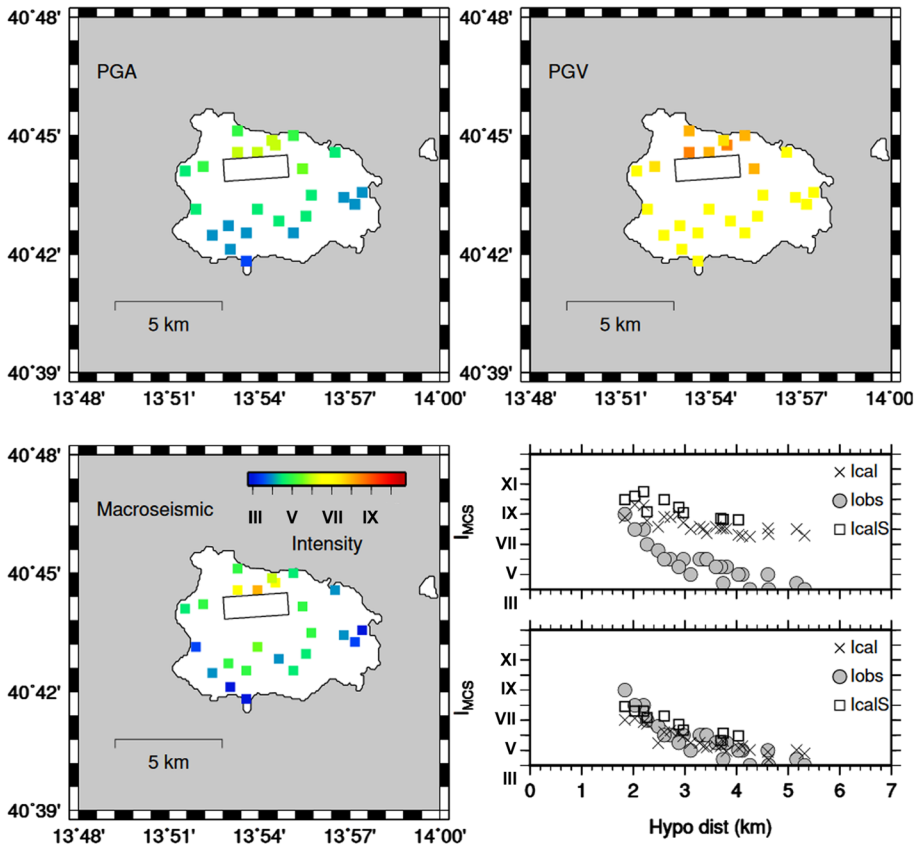
Fig. 3 Best model solution for the August 27, 2017, $M_w = 3.9$, earthquake. The lower left panel depicts the observed macroseismic data and the surface fault projection of the fault geometry proposed by De Novellis et al. (2018). The upper left panel shows the intensity values as obtained by converting PGAs in intensities, the upper right panel those obtained by using the PGVs. The lower right panels show the observed intensities as function of the hypocentral distance (grey circles), the computed intensities (crosses) and the computed intensities corrected by the site effects (squares) (upper for PGVs and lower for PGAs) (See also Table 1 model M1-A-V)

the opposite direction, at the same distance. This makes EXSIM procedure to prefer a slightly larger plane, with the centre shifted south-westward.

As for the 28 July 1883 earthquake, we used the observed macroseismic intensities obtained in the present study consisting in 26 data points with intensities ranging between VI and XI. The macroseismic epicentre obtained by using BOXER is 40.746°N (± 0.5 km) 13.893°N (± 1.2 km), the best azimuth 86° (± 30°), very similar to those resulting for the 2017 and 1881 events. The surface fault projection extent is an almost squared plane with dimensions 2.5×3.4 km², whose larger extension is the N-S direction. Following the same modelling strategy described above, we used EXSIM code and obtained the best models listed in Table 3 (MB83) and represented in Fig. 6. For this earthquake as well, PGA- and PGV-derived intensities indicate distinct values for all the parameters and, also in this case, the PGA simulation provides better fit to the data.
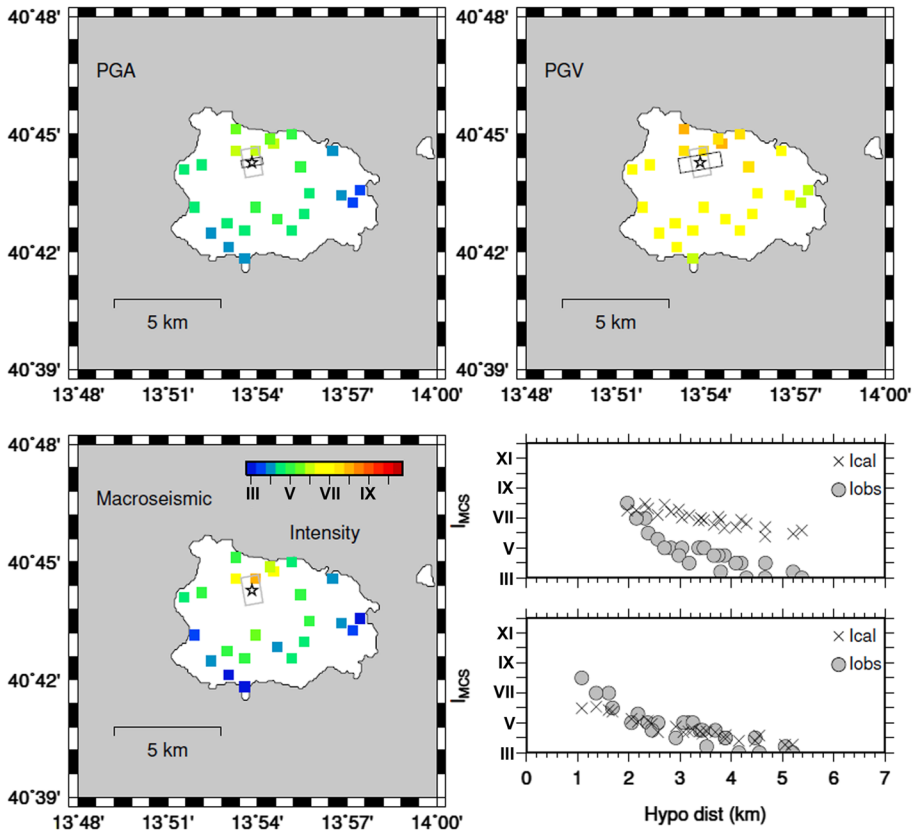
Fig. 4 Best model solution for the August 27, 2017, $M_W = 3.9$, earthquake for uniform slip distribution, using distinct fault reference points. The lower left panel depicts the observed macroseismic data and the surface fault projection obtained by using BOXER (grey box). The black star in all the panels identifies the macroseismic epicentre. The upper left panel shows the intensity values as obtained by converting PGAs in intensities and the inferred fault geometry (black box) (see Table 1), the upper right panel those obtained by using the PGVs. The lower right panels show the observed intensities as function of the hypocentral distance (grey circles) and the computed intensities (crosses) (upper for PGVs and lower for PGAs) (See also Table 1 model MB17-A-V)

The PGA best solution is associated with a 1×1 km^2 vertical plane, centred 500 m to the south and to the east with respect to the BOXER epicentre, while a 2×2 km^2 fault, dipping north 70°, results for PGV, with fault centre coincident with the BOXER one.

It should be remarked that, although associated with a higher magnitude, the 1883 fault dimension resulted to be smaller than 1881 but with the same stress drop. This result derives from the apparently different intensity distribution for the two events (Fig. 8, Appendix), displaying a definitely stronger gradient in the epicentral area for the 1883 (Fig. 2). We speculate that this might be related to differences in the slip distribution, possibly smoother for the 1881 earthquakes.

As for the maximum PGA and PGV values for the 1881 event, we obtain 6.7 m/s^2 (0.7 g) and 0.30 m/s, while for the 1883 event 14.3 m/s^2 (1.5 g) and 0.80 m/s, respectively. For both the events, the simulated PGA values, while reproducing the observed macroseismic intensities, significantly exceed the range of values (0.1, 0.2) g (corresponding to the 16th and 80th
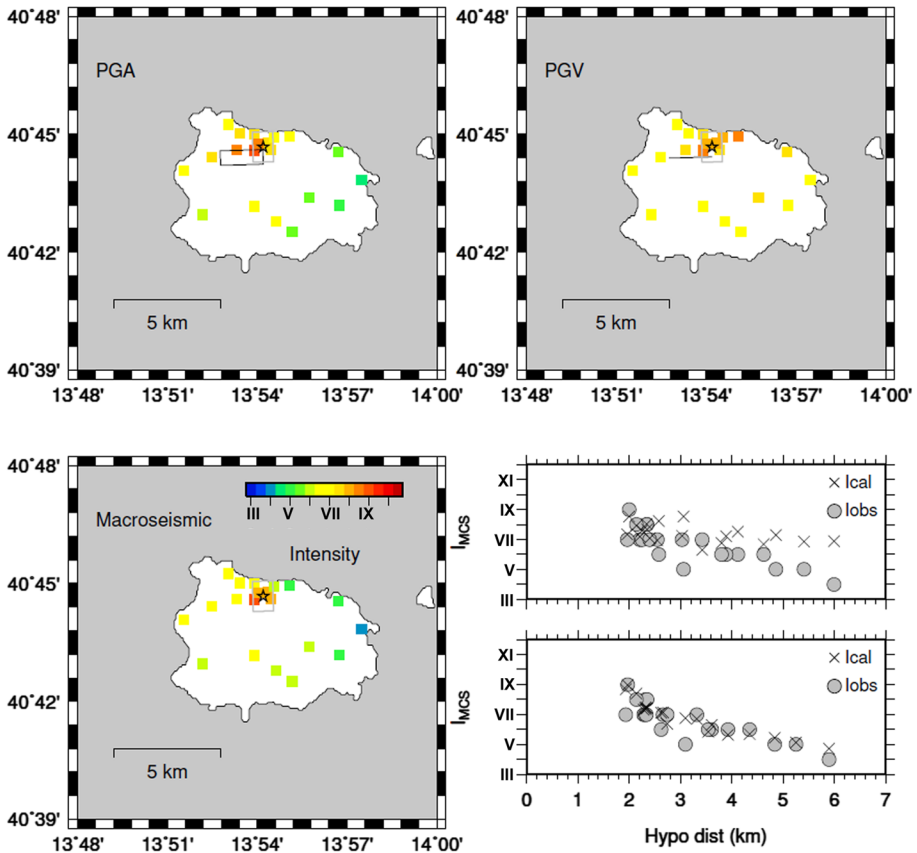
Fig. 5 Best model solution for the 4 March 1881, $M_W = 4.1$, earthquake for uniform slip distribution, using distinct fault reference points. The lower left panel depicts the observed macroseismic data and the surface fault projection obtained by using BOXER (grey box). The black star in all the panels identifies the macroseismic epicentre. The upper left panel shows the intensity values as obtained by converting PGAs in intensities and the inferred fault geometry (black box), the upper right panel those obtained by using the PGVs. The lower right panels show the observed intensities as function of the hypocentral distance (grey circles) and the computed intensities (crosses) (upper for PGVs and lower for PGAs) (See also Table 3 model MB81-A-V)

percentile, respectively) prescribed in the official hazard map as reference for the design of civil structures. It should be noted that the g values obtained from the PGA and PGV values are theoretical and also represent the maximum at the epicentre for the two historical events. In particular for the 1883 event, the g theoretical value is six times the value for the 2017 (0.25 g), recorded 800 m away from the epicentre, while the inferred magnitude is about 1 degree larger than the 2017 event.
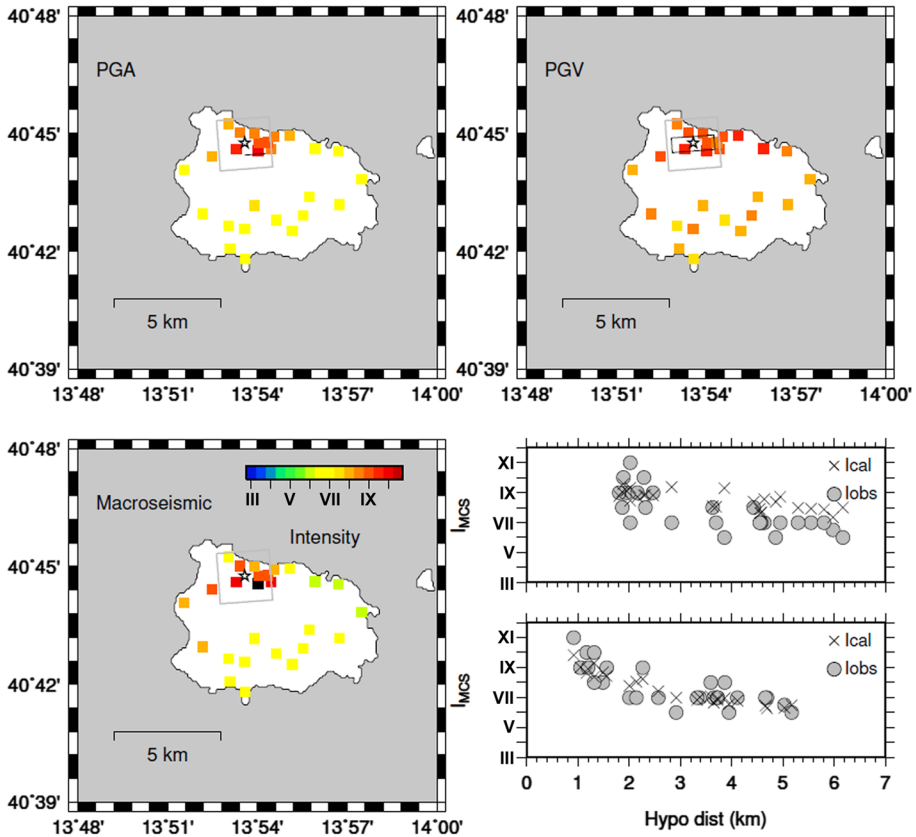
Fig. 6 Same as Fig. 3 but for the 28 July 1883, $M_W = 4.8$, earthquake. (See also Table 3 model MB83-A-V)

5 Discussion

The above elaborations indicate that the seismogenic sources associated with the 1881, 1883, and 2017 earthquakes are located along the northern rim of the Mt. Epomeo resurgent structure with strike roughly in the E-W direction. The fault dimensions resulting for the three events ranges between 1×1 km^2 and 2×2 km^2, associated with vertical or almost vertical planes, possibly dipping south. According to the island volcano-tectonics, the system of faults along the northern sector was moved with a thrust mechanism during the resurgence, while the latter was inverted as a normal one, during the subsidence phase (Acocella and Funiciello 1999; Acocella et al. 2001).

Considering the uncertainties in the intensity estimate—either for the observed data points or for the PGA and PGV converted values (± 0.35 and ± 0.26, respectively; Faenza and Michelini 2010)—and in the modelling procedure (propagation and site effects), we consider that, based on the available data, stress drop and Mach number estimates are hardly constrainable with a lower degree of uncertainty. On the other hand, also taking into account the local geology and independent results from analysis of the 2017 earthquake (De Novellis et al. 2018), we conclude that the results about the fault geometry and extent can be considered realistic and reliable within the sampling step of the parameters used in our analysis. The seismogenic source resulting from our study is compatible with the faults system bordering the northern rim of the resurgent structure.

The lateral extension of this fault system is structurally limited by the extension of the active part of the resurgent block, about 2 km in length (Acocella and Funiciello 1999; Carlino et al. 2006; Di Giuseppe et al. 2017; Sbrana and Toccaceli 2011). This limit encloses the fault plane (De Novellis et al. 2018) and the observed coseismic fractures (Nappi et al. 2018) of the 2017 events and seems to represent the maximum possible extent of seismogenic sources in the northern sector of the island. Moreover, the maximum depth at which the fragile shear failure can occur is limited by the brittle-ductile transition of rocks, which is located at a depth of about 2 km beneath the Mt. Epomeo (Carlino et al. 2012; Castaldo et al. 2017; Carlino 2018). This depth also corresponds to the cut-off depth of seismicity recorded in the island (D'Auria et al. 2018).

Furthermore, the macroseismic field for the 1881, 1883, and 2017 events shows that the most damaged areas for the three events have similar shape and are strikingly coincident (Fig. 7). The obtained 1881 and 1883 epicentre locations and that of 2017 are very close to each other, with maximum separation of ~ 600 m. These observations suggest a single seismic source as responsible for the destructive earthquakes of Ischia Island, whose reactivation is likely associated with a local stress field variation (Trasatti et al. 2020). The latter hypothesis is also supported by other observations: (i) the absence of significant (M > 1.5) seismic events outside the northern sector of the island; (ii) the absence of regional seismogenic structures crossing the island; (iii) the
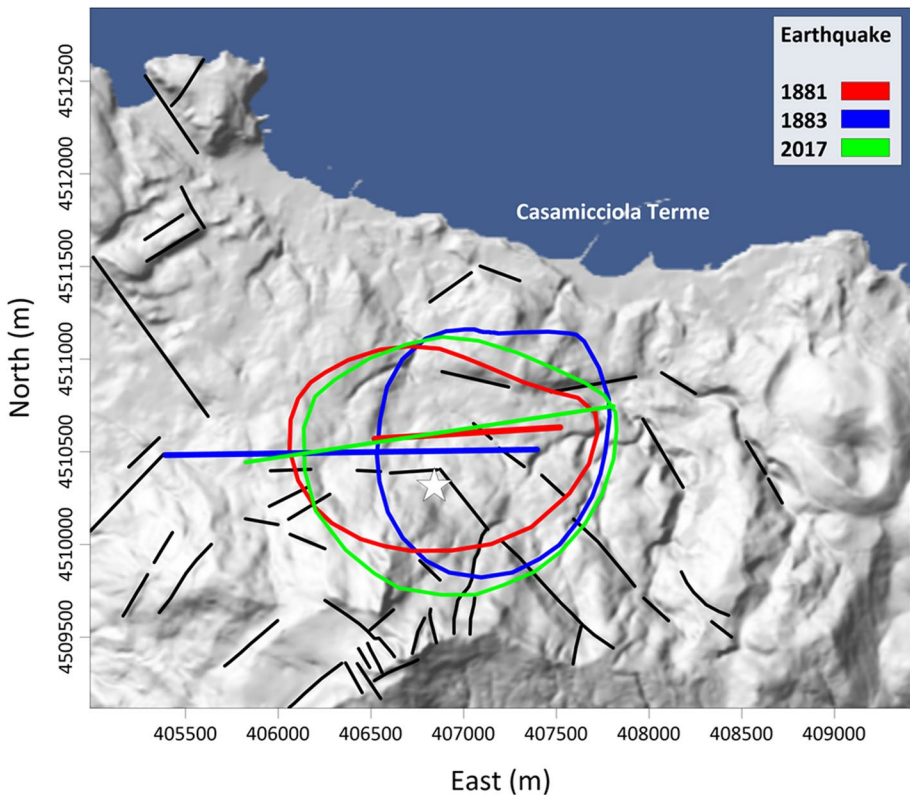

Fig. 7 Summary of results of this study. Circles represent the maximum isoseims of the earthquakes (I_0 VIII-IX 1881, I_0 X-XI 1883, and I_0 VII-VIII 2017) obtained from the interpolation of intensity data, while coloured lines are the surface projection of the fault plane solutions obtained from EXSIM (blue and red) and from De Novellis et al. (2018) (green). White star is the instrumental epicentre of 2017 event

occurrence of very few aftershocks associated with the 2017 event (less than 30) and localized along the slipped zone (De Novellis et al. 2018); (iv) the presence of faults system around the Mt. Epomeo structure, which does not show a preferential regional pattern orientation, and whose formation is associated with the resurgence process and to the progressive failure of the brittle curst (Sbrana et al. 2009; Carlino 2012; Di Giuseppe et al. 2017).

On the basis of the above observations and of the result of the simulations, the seismogenic fault of 1881 and 1883 does not exceed 2×2 km^2. Given that this source area is actually confined by the structural evolution of Mt. Epomeo and the brittle-ductile transition below the island, we suggest that this specific seismogenic fault can provide a magnitude that is unlikely to exceed the range 5.0 ± 0.3, assuming empirical relations between rupture area and magnitude (Wells and Coppersmith 1994; Somerville et al. 1999).

Furthermore, the results obtained from the BOXER and EXSIM elaborations, which agree with a roughly E-W strike of the seismogenic fault, locate this latter along the most strained zone of the Mt. Epomeo (Acocella and Funiciello 1999), where the maximum load of the resurgent block is exerted during the present subsidence phase. The subsidence possibly took place since ancient Roman Age at least (Buchner et al. 1996), therefore the historical earthquakes likely occurred in a geodynamic context similar to the present one. This makes the vertical loading of the Mt. Epomeo the predominant stress (σ_1) of the area (Manzo et al. 2006; De Martino et al. 2011; Castaldo et al. 2017; De Novellis et al. 2018; Trasatti et al. 2020). Moreover, the minimum tensional stress acting at regional scale, is approximately NNW-SSE oriented (Hippolyte et al. 1994), favouring normal faulting along the roughly E-W seismogenic structure of the north of Mt. Epomeo (Lowrie 2007; Zoback 2010).

As regards the causes of the subsidence, two possible main processes have been suggested in the recent literature. The first process could be associated with the depressurization of a shallow magmatic system (Trasatti et al. 2020), the second one foresees the persistence of a stress field associated with the loading of Mt. Epomeo, and the coupling action of volcano loading and crust rheology (Castaldo et al. 2017; De Novellis et al. 2018). For both scenarios, the subsidence of the Mt. Epomeo represents the mechanism that accumulated strain energy along the seismic fault and for which only normal fault mechanism can occur.

6 Conclusions

In this study, we attempted at reassessing the location and magnitude of two important historical earthquakes of Ischia Island (1881 and 1883) and their possible relation with the recent 21 August 2017 event. We analysed the available macroseismic data and derived quantitative information about the source parameters of the three earthquakes, verifying the similarities of their seismic sources. Although intrinsic approximations and uncertainties are associated with the adopted procedure, the results obtained initially by modelling the data of the 2017 earthquake validates our approach, demonstrating its effectiveness in retrieving consistent information on the source of earthquakes in the northern sector of Ischia Island from macroseismic data. Our results suggest that:

- a single seismogenic structure is likely to be responsible for the known destructive earthquakes on the island, located on the northern slope of Mt. Epomeo. The plane has a roughly E-W strike, it is dipping vertically or possibly southwards at high angle, as already evidenced by Acocella et al. (1999) from geological survey and by De Novellis et al. (2018) and Trasatti et al. (2020) for the 21 August 2017 event;

- the data of both historical and recent earthquakes, joined with geological and geophysical information, indicate a fault dimension of about 2×2 km^2. The maximum magnitude for earthquakes in the northern sector Ischia Island cannot exceed ~5.0;
- the magnitude of the 1881 and of the 1883 events are evaluated around 4.1 and 4.8, respectively, with the latter value possibly affected by cumulative damage;
- the simulated PGA values for the 1881 and 1883 events significantly exceed the PGA values, also referring to the 84th percentile, with probability of exceeding equal to 10% in 50 years reported in the official national seismic hazard map.

We cannot exclude that further seismogenic sources can be activated in the island, although this appears an unlikely scenario, in consideration of the thickness of the fragile crust (which is larger in the northern sector of the island) (Carlino et al. 2006) and of the structural dynamic of Mt. Epomeo. Finally, this work highlights the complexity of the processes leading to the seismic energy accumulation and release in such resurgent calderas and the necessity of refining the national seismic hazard map at a smaller local scale—possibly using a single fault-based approach—and integrating recorded and simulated PGA and PGVs values.

Appendix
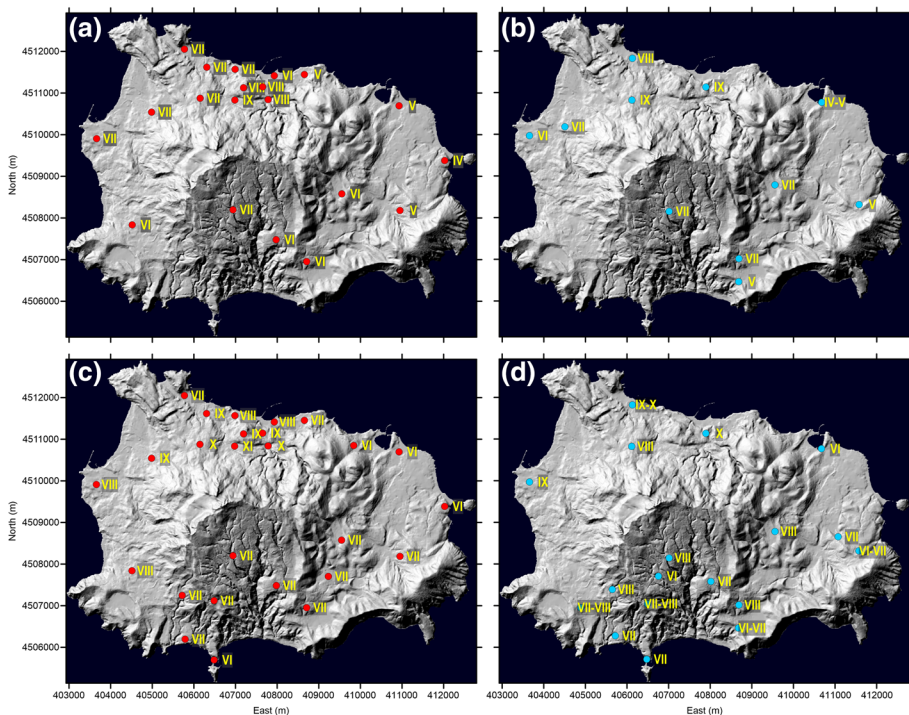
See Fig. 8.
See Tables 4, 5 and 6

Fig. 8 Comparison of location and distribution of intensity points obtained from this study (**a** and **c**) and reported in the CPTI15 (Rovida et al. 2019) (**b** and **d**)

Table 4 Historical seismicity in the island of Ischia as reported by Cubellis and Luongo, (1998)

Year	Epicentral area	Epicentral intensity MCS	Magnitude	Damages
1228	CASAMICCIOLA	IX-X*	–	700 deaths, large landslide from Mt. Epomeo
1275	NORTHERN SECTOR	VIII-IX (VIII-IX)	– (4.0)	Damages
1302	EASTERN AREA	VIII	–	Many buildings collapse
1557	SOUTHEAST AREA	VII-VIII (VI-VII)	– (3.5)	Collapse of the Parish Church
1762	CASAMICCIOLA	VII (VI-VII)	– (3.5)	Damage to houses in Casamicciola
1767	EASTERN AREA	VII-VIII (VI-VII)	– (3.5)	Collapse of Rotaro's Church
1769	CASAMICCIOLA	VIII	–	7 deaths, serious damage in the upper part of Casamicciola
1828	CASAMICCIOLA	VIII-IX (VIII-IX)	– (4.0)	28 deaths, 50 injured, serious damage and collapses in the upper part of Casamicciola
1841	CASAMICCIOLA	VII (V-VI)	– (3.3)	Cracks in the buildings
1863	CASAMICCIOLA	VII (VI-VII)	– (4.9)	Collapse of dry walls, small landslides from Mt. Epomeo
1867	CASAMICCIOLA	VI-VII (IV-V)	– (3.0)	Buildings damaged at Casamicciola
1881	CASAMICCIOLA	IX (IX)	– (4.1)	129 deaths, many injured, many collapsed buildings at Casamicciola and Lacco Ameno
1883	CASAMICCIOLA	XI (IX-X)	4.6–5.2 (4.3)	2333 deaths, 762 injured, many collapsed at Casamicciola, Lacco Ameno and Forio

Epicentral intensity and magnitude values from CPTI15 (Rovida et al., 2019) have been added in parentheses

*Uncertain earthquake

Table 5 Intensity data for the 1881 earthquake obtained in this work (see main text for details). Coordinates are UTM (zone 33 N)

33 N easting	33 N northing	Intensity (EMS)	Locality
406,979.55545145	4,510,832.1986336	IX	Maio-Casamennella-Montecito
407,189.79128191	4,511,127.873485	VIII	Sentinella
407,651.45549307	4,511,149.3144697	VIII	Margherita
407,782.65268468	4,510,842.839224	VIII	Bagni
403,660.33735065	4,509,906.350412	VII	Forio
404,980.5725428	4,510,542.3354071	VII	Baiola
405,773.51537075	4,512,053.529341	VII	Marina-S. Montano
406,150.59852408	4,510,876.3822858	VII	Fango
406,307.71946561	4,511,617.8779215	VII	Lacco est
406,939.30472379	4,508,198.3741856	VII	Fontana
406,987.02980633	4,511,571.238704	VII	Marina ovest
404,518.12442628	4,507,833.5387983	VI	Panza
407,927.92532303	4,511,419.1542994	VI	Marina
407,975.54139937	4,507,477.9861258	VI	Buonopane-Terzano
408,710.51160602	4,506,953.1679507	VI	Barano-Testaccio
409,553.36734758	4,508,577.9128686	VI	Fiaiano
408,655.90267324	4,511,447.5433883	V	Perrone
410,926.37935059	4,510,696.8522028	V	Ischia porto
410,951.66502284	4,508,180.9278143	V	Campagnano
412,023.77752611	4,509,379.4686788	IV	Ponte

Table 6 Intensity data for the 1883 earthquake obtained in this work (see main text for details). Coordinates are UTM (zone 33 N)

33 N easting	33 N northing	Intensity MCS	Locality
406,977	4,510,831	XI	Maio-Casamennella-Montecito
407,783.30811481	4,510,838.0519914	X	Bagni
406,146.72233829	4,510,874.9986406	X	Fango
407,190.34445716	4,511,128.3819839	IX	Sentinella
407,651.84189878	4,511,148.3731966	IX	Margherita_est
406,306.58656741	4,511,618.2759022	IX	Lacco_est
404,983.01943954	4,510,543.977835	IX	Baiola
407,929.3553968	4,511,417.1853011	VIII	Marina
406,983.96338296	4,511,570.4740082	VIII	Marina_ovest
404,512.2115859	4,507,839.9275328	VIII	Panza
403,657.32295363	4,509,910.8644273	VIII	Forio
408,654.0933111	4,511,455.3249717	VII	Perrone
405,773.00819576	4,512,049.8371005	VII	Marina-S.Montano
406,941.84527635	4,508,199.9204528	VII	Fontana
406,482.27952837	4,507,120.1490408	VII	Serrara
405,789.9335643	4,506,193.5714781	VII	Succivo
405,718.87355089	4,507,245.9917786	VII	Ciglio
408,712.04139946	4,506,953.7704396	VII	Barano-Testaccio
407,978.64920513	4,507,484.1817893	VII	Buonopane-Terzano
409,549.70049883	4,508,576.523612	VII	Fiaiano
409,229.9355335	4,507,700.7609321	VII	Piedimonte-Casabona
410,950.53303198	4,508,185.5648735	VII	Campagnano
406,483.19002899	4,505,694.5479251	VI	S.Angelo
410,927.53023529	4,510,698.956571	VI	Ischia_porto
409,838.69560846	4,510,850.696791	VI	Quercia
412,022.81857414	4,509,385.7740881	VI	Ponte

Availability of data and materials The data of 1883 earthquake used in this paper came from published sources listed in the references. The data of 1881 earthquake are in part inferred from unpublished data collected from the historical archive of Naples. Some plots were made using the Generic Mapping Tools version 5.4.5 (www.soest.hawaii.edu/gmt; Wessel and Smith 1998).

Declarations

Conflict of interest The authors declare that they have no conflict of interest.

Consent to participate The authors declare that this research would be used only for scientific research and would not passed on to third parties.

Consent for publication The authors authorize the publication of this manuscript.

References

Acocella V, Funiciello R (1999) The interaction between regional and local tectonics during resurgent doming: the case of the island of Ischia, Italy. J Volc Geotherm Res 88:109–123

Acocella V, Cifelli F, Funiciello F (2001) The control of overburden thickness on resurgent domes: insights from analogue models. J Volc Geotherm Res 111:137–153

Akinci A, Galadini F, Pantosti D, Petersen M, Malagnini L, Perkins D (2009) Effect of time dependence on probabilistic seismic-hazard mapsand deaggregation for the central apennines, Italy. Bull Seism Soc Am 99:585–610

Assatourians K, and Atkinson G (2012) EXSIM12: A Stochastic Finite-Fault Computer Program in FORTRAN, http://www.seismotoolbox.ca (last accessed November 2014).

Atkinson G, Assatourians K (2014) Implementation and validation of EXSIM (A stochastic finite-fault ground-motion simulation algorithm) on the SCEC broadband platform. Seismol Res Lett 86:48–60

Azzaro R, D'Amico S, Tuvè T (2011) Estimating the magnitude of historical earthquakes from macroseismic intensity data: new relationships for the volcanic region of Mount Etna (Italy). Seismol Res Lett 82:533–544

Boore DM (2009) Comparing stochastic point-source and finite-source ground-motion simulations: SMSIM and EXSIM. Bull Seism Soc Am 99:3202–3216

Braun T, Famiani D, Cesca S (2018) Seismological constraints on the source mechanism of the damaging seismic event of 21 August 2017 on Ischia Island (Southern Italy). Seismol Res Lett 89:1741–1749

Briseghella B, Demartino C, Fiore A, Nuti C, Sulpizio C, Vanzi I, Lavorato D, Fiorentino G (2019) Preliminary data and field observations of the 21st August 2017 Ischia earthquake. Bull Earthq Eng 17(3):1221–1256

Buchner G, Italiano A, Vita-Finzi C (1996) Recent uplift of Ischia, southern Italy. Geol Soc, London, Spec Publ 110:249–252

Calderoni G, Di Giovambattista R, Pezzo G, Albano M, Atzori S, Tolomei C, Ventura G (2019) Seismic and Geodetic Evidences of a Hydrothermal Source in the Md 4.0, 2017, Ischia earthquake (Italy). J Geophys Res 124:5014–5029

Capuano P, De Matteis R, Russo G (2015) The structural setting of the Ischia Island Caldera (Italy): first evidence from seismic and gravity data. Bull Volcanol 77:79

Carlino S (2012) The process of resurgence for Ischia Island (southern Italy) since 55 ka: the laccolith model and implications for eruption forecasting. Bull Volcanol 74:947–961

Carlino S (2018) Heat flow and geothermal gradients of the Campania region (Southern Italy) and their relationship to volcanism and tectonics. J Volc Geotherm Res 365:23–37

Carlino S (2019) Volcanoes and Human Settlements. In *Neapolitan Volcanoes* (pp. 115–178). Springer, Cham.

Carlino S, Cubellis E, Luongo G, Obrizzo F (2006) On the mechanics of caldera resurgence of Ischia Island (southern Italy). Geol Soc, London, Spec Publ 269:181–193

Carlino S, Cubellis E, Marturano A (2010) The catastrophic 1883 earthquake at the island of Ischia (southern Italy): macroseismic data and the role of geological conditions. Nat Hazards 52:231

Castaldo R, Gola G, Santilano A, De Novellis V, Pepe S, Manzo R, Manzella A, Tizzani P (2017) The role of thermo-rheological properties of the crust beneath Ischia Island (Southern Italy) in the modulation of the ground deformation pattern. J Volc Geotherm Res 344:154–173

Comitato Centrale di Soccorso pei Danneggiati dell'Isola d'Ischia (1885) *Relazione*, Giannini e Figli. Archivio di Stato di Napoli, Napoli

Convertito V, Pino NA (2014) Discriminating among distinct source models of the 1908 Messina Straits earthquake by modelling intensity data through full wavefield seismograms. Geophys J Int 198:164–173

Convertito V, Zollo A (2011) Assessment of pre-crisis and syn-crisis seismic hazard at Campi Flegrei and Mt. Vesuvius volcanoes, Campania, southern Italy. Bull Volcanol 73:767–783

Convertito V, Emolo A, Zollo A (2006) Seismic hazard assessment for a characteristic earthquake scenario: an integrated probabilistic–deterministic method. Bull Seism Soc Am 96:377–391

Convertito V, Caccavale M, De Matteis R, Emolo A, Wald DJ, Zollo A (2012) Fault extent estimation for near-real time ground-shaking map computation purposes. Bull Seismol Soc Am 102:578–586

Crescimbene M, La Longa F, Camassi R, Pino NA (2015) The seismic risk perception questionnaire, Geological Society, London, Special. Publication 419:69–77

Cubellis E, and Luongo G (1998) Il terremoto del 28 luglio 1883. Danni, vittime ed effetti al suolo, in "Il terremoto del 28 luglio 1883 a Casamicciola nell'Isola d'Ischia", Istituto Poligrafico e Zecca dello Stato, Roma 59–100.

Cubellis E, Carlino S, Iannuzzi R, Luongo G, Obrizzo F (2004) Management of historical seismic data using GIS: the island of Ischia (Southern Italy). Nat Hazards 33:379–393

D'Auria L, Giudicepietro F, Tramelli A, Ricciolino P, Lo Bascio D, Orazi M, Martini M, Peluso R, Scarpato G, Esposito A (2018) The seismicity of Ischia Island. Seismol Res Lett 89:1750–1760

De Martino P, Tammaro U, Obrizzo F, Sepe E, Brandi G, D'Alessandro A, Dolce M, and Pingue F (2011) La rete GPS dell'isola d'Ischia: Deformazioni del suolo in un'area vulcanica attiva (1998–2010), Quaderni di Geofisica **95**.

De Natale G, Iannaccone G, Martini M, Zollo A (1987) Seismic sources and attenuation properties at the Campi Flegrei volcanic area, Pure Appl. Geophys 125:883–917

De Natale G, Faccioli E, Zollo A (1988) Scaling of peak ground motions from digital recordings of small earthquakes at Campi Flegrei, southern Italy, Pure Appl. Geophys 126:37–53

De Natale G, Petrazzuoli S, Romanelli F, Troise C, Vaccari F, Somma R, Peresan A, Panza G (2019) Seismic risk mitigation at Ischia island (Naples, Southern Italy): An innovative approach to mitigate catastrophic scenarios. Eng Geol 261:1–10

De Novellis V, Carlino S, Castaldo R, Tramelli A, De Luca C, Pino NA, Pepe S, Convertito V, Zinno I, De Martino P, Bonano M, Giudicepietro F, Casu F, Macedonio G, Manunta M, Cardaci C, Manzo M, Di Bucci D, Solaro G, Zeni G, Lanari R, Bianco F, Tizzani P (2018) The 21 August 2017 Ischia (Italy) earthquake source model inferred from seismological, GPS, and DInSAR measurements. Geophys Res Lett 45:2193–2202

Del Pezzo E, Bianco F (2013) A reappraisal of seismic Q evaluated in Campi Flegrei caldera. Receipt for the application to risk analysis. J Seismol 17:829–837

Del Gaudio C, Di Domenico M, Ricci P, Verderame GM (2018) Preliminary prediction of damage to residential buildings following the 21st August 2017 Ischia earthquake. Bull Earthq Eng 16:4607–4637

Di Giuseppe MG, Troiano A, Carlino S (2017) Magnetotelluric imaging of the resurgent caldera on the island of Ischia (southern Italy): inferences for its structure and activity. Bull Volcanol 79:85

Faenza L, Michelini A (2010) Regression analysis of MCS intensity and ground motion parameters in Italy and its application in ShakeMap. Geophys J Int 180:1138–1152

Gasperini P, Ferrari G (2000) Deriving numerical estimates from descriptive information: the computation of earthquake parameters. Ann Geophys 43:729–746

Gasperini P, Bernardini F, Valensise G, Boschi E (1999) Defining seismogenic sources from historical felt reports. Bull Seism Soc Am 89:94–110

Gasperini P, Vannucci G, Tripone D, Boschi E (2010) The location and sizing of historical earthquakes using the attenuation of macroseismic intensity with distancelocation and sizing of historical earthquakes using attenuation of macroseismic intensity. Bull Seism Soc Am 100:2035–2066

Grünthal G (ed) (1998) European Macroseismic Scale 1998 (EMS-98), Cahiers du Centre Européen de Géodynamique et de Séismologie, **15**. Centre Européen de Géodynamique et de Séismologie, Luxembourg, p 99

Kerry KE, Hawick KA (1998) Kriging interpolation on high-performance computers. In: Sloot P et al (eds) High-Performance Computing and Networking. HPCN-Europe, Springer, Berlin, Heidelberg, pp 429–438

Locati M, Camassi R, Rovida A, Ercolani E, Bernardini F, Castelli F, Caracciolo C H, Tertulliani A, Rossi A, Azzaro R, D'Amico S, Conte S, Rocchetti E, and Antonucci A (2019). Database Macrosismico Italiano (DBMI15), versione 2.0., Istituto Nazionale di Geofisica e Vulcanologia (INGV).

Lowrie W (2007) Fundamentals of Geophysics, 2nd edn. Cambridge University Press, New York, p 381

Mai M, Spudich P, Boatwright J (2005) Hypocenter locations in finite-source rupture models. Bull Seism Soc Am 95:965–980

Manzo M, Ricciardi GP, Casu G, Ventura G, Zeni G, Borgström S, Berardino P, Del Gaudio C, Lanari R (2006) Surface deformation analysis in the Ischia Island (Italy) based on spaceborne radar interferometry. J Volc Geotherm Res 151:399–416

Marotta A, Liberatore D, Sorrentino L (2019) Historical Building Codes issued after the strong Italian earthquakes of Norcia (1859) and Ischia (1883). Ann Geophys 62(3):337

Marturano A, Esposito E, Porfido S, and Luongo G (1988) Il terremoto del 4.10.1983 (Pozzuoli). Attenuazione delle intensità con la distanza e relazione magnitudo-intensità: Zonazione della città di Napoli, Atti 74° Congresso Naz. Soc. Geol. It., Sorrento 13–17 settembre 1988, 303–311.

McNutt SR, Roman DC (2015) Volcanic seismicity. The Encyclopedia of Volcanoes. Academic Press, New York, pp 1011–1034

Molnar P (1979) Earthquake recurrence intervals and plate tectonics. Bull Seism Soc Am 69:115–133

Motazedian D, Atkinson GM (2005) Stochastic finite-fault modeling based on a dynamic corner frequency. Bull Seism Soc Am 95:995–1010

Musson RMW, and Jiménez MJ (2008) Macroseismic estimation of earthquake parameters, NERIES project report, Module NA4, Deliverable D3, Edinburgh.

Musson RMW, Grünthal G, Stucchi M (2010) The comparison of macroseismic intensity scales. J Seismol 14:413–428

Nappi R, Alessio G, Gaudiosi G, Nave R, Marotta E, Siniscalchi A, Civico R, Pizzimenti L, Peluso R, Belviso P, Porfido S (2018) The 21 August 2017 M d 4.0 Casamicciola earthquake: First evidence of coseismic normal surface faulting at the Ischia volcanic island. Seismol Res Lett 89:1323–1334

Nazeri S, Zollo A, Adinolfi GM, Amoroso O, Picozzi M (2020) The 2017, Mw 3.9 Ischia Earthquake (Southern Italy): Source mechanism from the modelling of seismic, geodetic, and geological data and relation to the volcano resurgence mechanism. J Geoph Res. https://doi.org/10.1002/essoar. 10504375.1

Nunziata C, Rapolla A (1987) A gravity and magnetic study of the volcanic island of Ischia, Naples (Italy). J Volc Geotherm Res 31:333–344

Pace B, Peruzza L, Lavecchia G, Boncio P (2006) Layered seismogenic source model and probabilistic seismic-hazard analyses in central Italy. Bull Seismic Soc Am 96:107–132

Panza GF, Cuscito M (1982) Influence of focal mechanism on shape of isoseismals: Irpinia earthquake of November 23, 1980, Pure Appl. Geophys 120:577–582

Patanè G, Imposa S, Gresta S, and Patanè D (1986) Rischi derivanti da eventi eruttivi e sismici nell'area etnea, Atti 5° Congresso Gruppo Nazionale di Geofisica della Terra Solida, Roma, 123–136.

Petrosino S, De Siena L, Del Pezzo E (2008) Recalibration of the magnitude scales at Campi Flegrei, Italy, on the basis of measured path and site and transfer functions. Bull Seism Soc Am 98:1964–1974

Polverino F (1996) Gli edifici antisismici nel patrimonio edilizio ischitano alla fine del XIX secolo. Elementi per la conservazione e la riqualificazione, in La Rassegna d'Ischia, **3**

Polverino F (1998) Ischia. Architettura e Terremoto, Clean edizioni, Napoli, p 252

Rovida A, Locati M, Camassi R, Lolli B, and Gasperini P (2019) Catalogo Parametrico dei Terremoti Italiani (CPTI15), versione 2.0., Istituto Nazionale di Geofisica e Vulcanologia (INGV).

Sbrana A, Toccaceli RM (eds) (2011) Carta Geologica Isola d'Ischia. Note illustrative, Regione Campania, Assessorato Difesa del Suolo, LAC Firenze

Sbrana A, Fulignati P, Marianelli P, Boyce AJ, Cecchetti A (2009) Exhumation of an active magmatic–hydrothermal system in a resurgent caldera environment: the example of Ischia (Italy). J Geol Soc 166:1061–1073

Seekins LC, Boatwright J (2010) Rupture directivity of moderate earthquakes in Northern California. Bull Seismol Soc Am 100:1107–1119

Somerville P, Irikura K, Graves R, Sawada S, Wald D, Abrahamson N, Iwasaki Y, Kagawa T, Smith N, Kowada A (1999) Characterizing crustal earthquake slip models for the prediction of strong ground motion. Seismol Res Lett 70:59–80

Tertulliani A, Arcoraci L, Berardi M, Bernardini F, Brizuela B, Castellano C, Del Mese S, Ercolani E, Graziani L, Maramai A, Rossi A, Sbarra M, Vecchi M (2012) The Emilia 2012 sequence: a macroseismic survey. Ann Geophys 55:679–687

Trasatti E, Acocella V, Di Vito MA, Del Gaudio C, Weber G, Aquino I, Caliro S, Chiodini G, de Vita S, Ricco C, Caricchi L (2020) Magma degassing as a source of long-term seismicity at volcanoes: The Ischia island (Italy) case. Geophys Res Lett 46:14421–14429

Vassallo M, Galluzzo D, Sapia V, Nardone L, Pischiutta M, Petrosino S, Bobbio A, Cara F, Carandente A, Civico R, Cogliano R, Cultrera G, Cusano P, De Vita S, Di Giulio G, Di Vito M, Esposito R, Famiani D, Giannattasio F, Marchetti M, Marotta E, Milana G, Moretti M, Napolitano F, Pucillo S, Riccio G, Sepe V, Tarabusi G, and Tramelli A (2018) Seismological and geophysical studies for

site effect characterization following the 2017 M_w=3.9 Ischia earthquake, in Abstract volume of the International meeting "Cities on volcanoes 10", Miscellanea INGV, **43** 565.

Verderame G M, Di Domenico M, Del Gaudio C, and Ricci P (2017) Rapporto relativo ad una preliminare predizione del danno agli edifici residenziali di Casamicciola Terme e Lacco Ameno a seguito del sisma del 21.08. 2017, ore 20.57, M=4.0, Technical Report.

Vezzoli L (ed.) (1988) Island of Ischia, *C.N.R.* Quaderni de "La Ricerca scientifica" **114** 135, Rome, 135 pp.

Wells DL, Coppersmith KJ (1994) New empirical relationships among magnitude, rupture length, rupture width, rupture area, and surface displacement. Bull Seismol Soc Am 84:974–1002

Wessel P, Smith WHF (1998) New, improved version of the generic mapping tools released. EOS Trans AGU 79:579

Zahradnik J (1989) Simple method for combined studies of macroseismic intensities and focal mechanisms, Pure Appl. Geophys 130:83–97

Zoback MD (2010) Reservoir geomechanics. Cambridge University Press, New York

Zobin VM (2012) Introduction to volcanic seismology. Elsevier, Amsterdam-New York-Tokyo, p 474

Publisher's Note Springer Nature remains neutral with regard to jurisdictional claims in published maps and institutional affiliations.